Polymer Testing 127 (2023) 108198

Contents lists available at ScienceDirect

Polymer Testing

journal homepage: www.elsevier.com/locate/polytest

A new technique to measure the dynamic fracture toughness of solids

Junyi Zhou [a], Antonio Pellegrino [a,**], Vito L. Tagarielli [b,*]

[a] Department of Engineering Science, University of Oxford, Oxford, OX1 3PJ, UK
[b] Department of Aeronautics, Imperial College London, London, SW72AZ, UK

ARTICLE INFO

Keywords:
Toughness
Dynamic fracture
Strain rate sensitivity
PMMA

ABSTRACT

We propose and assess a new experimental technique to measure the fracture toughness of engineering materials and its sensitivity to strain rate. The proposed method is based on a ring expansion technique and it overcomes the limitations of current dynamic fracture tests, as it is not affected by transient stress wave propagation during loading and it results in spatially uniform remote stress and strain fields prior to fracture; the method is also suitable to achieve remote strain rates well in excess of 1000 s^{-1}. We demonstrate the technique by measuring the plane-stress Mode I fracture toughness of PMMA specimens at remote strain rates ranging from 10^{-3} s^{-1} to 10^{2} s^{-1}. The experiments show an increase of the toughness of the material with increasing strain rate.

1. Introduction

We aim at addressing the difficulties in measuring the dynamic fracture response of engineering solids. This study focuses on PMMA due to its ready availability, ease of manufacturing and to the attention received by this material in the published literature (see for example [1–3]); however, the technique presented in this paper is applicable to any solid that can be manufactured in the form of thin-walled rings.

The literature on dynamic fracture testing of solids is very vast [4]. For the case of PMMA for example, researchers have induced dynamic fracture using different techniques, such as drop-weight loading of unsupported plates [5] or simply supported beams in three-point bending [6], Split Hopkinson Pressure bar (SHPB) loading of beams in bending [7,8] or of cracked Brazilian disk specimens [9]. Dynamic testing of engineering materials in general has been conducted by extending quasi-static test protocols to the dynamic loading regime. This has involved subjecting to impulsive loading CT specimens, notched beams, double cantilever specimens, cracked strips or dogbone specimens [4]. All these techniques have problematic aspects in common.

- They involve the transient propagation of stress waves, resulting in time-dependent stress-intensity factors whose determination is very difficult, particularly in materials with complex architectures.
- A remote applied strain rate cannot be adequately defined (with the exception of direct tension tests on cracked strips or dogbone specimens).
- The strain rates achievable in practice are generally low.

Some recent developments in the testing of brittle materials like rock have shown that notched semi-circle bend (NSCB) specimens can be tested in a SHPB to determine the dynamic fracture toughness [10,11], however such specimens are subject to a non-uniform strain field during loading, such that a remotely applied strain rate is difficult to identify.

A test technique that received relatively little attention by the dynamic fracture community is ring expansion, where a thin-walled ring-shaped specimen is internally or externally pressurised to induce a circumferential stress. Much of these tests used explosives or ballistic impact [12–14] or electromagnetic forces [15–18] as a mean to generating suitable loading pulses. The above tests were demonstrated on ductile materials (metals in most cases) and did not allow measurements of stress versus strain curves, which are in high demand by the modelling community. For brittle materials, in Ref. [19] a SHPB and a hydraulic based apparatus was employed to perform compression and tension tests on thick-walled cylindrical rock specimen.

We have recently explored the application of such technique with the objective of obtaining valid tensile stress versus strain curves for a variety of solids of engineering interest. In Refs. [20–23] we showed that this technique is effective in quasi-static and dynamic scenarios, that it can be applied in controlled environmental conditions, and can be used to conduct tensile tests at strain rates as high as 5000 s^{-1}. In this study we illustrate the application of the ring expansion technique to the case of cracked specimens, with the objective of measuring the dynamic

* Corresponding author.
** Corresponding author.
E-mail addresses: antonio.pellegrino@eng.ox.ac.uk (A. Pellegrino), v.tagarielli@imperial.ac.uk (V.L. Tagarielli).

https://doi.org/10.1016/j.polymertesting.2023.108198
Received 5 March 2023; Received in revised form 1 August 2023; Accepted 7 September 2023
Available online 11 September 2023

fracture toughness of solids at well-defined applied strain rates. We note that this technique addresses the limitations of the other tests listed above: it results (to a very good approximation) in spatially uniform remotely applied stress and strain field, and in a remotely applied strain rate which can be clearly defined and measured, and it can be chosen to be very high. In addition, no complex strain diagnostics (such as high-speed photography, digital image correlation) or accompanying numerical simulations are required to interpret the test data, resulting in relatively inexpensive experiments which can be conducted with a standard SHPB apparatus.

In the following we illustrate the details of the technique and present and discuss our dynamic toughness measurements on PMMA specimens.

2. Materials and experimental technique

2.1. specimens

Ring specimens were manufactured from an extruded PMMA bar to have internal diameter $D = 50$ mm, wall thickness $t = 1$ mm and height $H = 5$ mm. One of such specimens is shown in Fig. 1a. An edge crack, oriented along the height direction, was manufactured by inducing a notch via a rotary machining tool (Dremel 3000) with a blade of 0.1 mm thickness, introducing a notch tip radius of approximately 30 μm. The depth of the notch, taken as the initial crack length, was measured (with precision of 10 μm) by observation in an optical microscope, as illustrated in Fig. 1b. In selected experiments a strain gauge of type FLK-10-23 (produced by Tokyo Measuring Instruments) was adhered to the specimen at a location opposite to that of the crack, oriented in the circumferential direction.

2.2. Test apparatus and its working principle

A schematic view of the apparatus is presented in Fig. 2a with the leading geometric dimensions (we refer the reader to Refs. [20,21] for further details of its geometry). This comprised two stainless steel plates connected by four hollow cylinders to form a metallic frame; the function of the frame is to resist the axial force exerted by the pressurised fluid during the test. The frame supported two pairs of metallic cylinder/piston pairs, sandwiching a 3D-printed rubber sleeve (Fig. 2b), on which the specimen (shown in red in Fig. 2a) was mounted. The chamber formed by the inner surface of the rubber sleeve, pistons and metal cylinders was filled with fluid (water in this case). By applying compressive loading to the pistons, using a standard tensometer (for quasi-static tests) or a SHPB (in dynamic tests), the water was pressurised, and this pressure induced radial expansion of the rubber sleeve and specimen.

Quasi-static tests (0.001 s^{-1}) were performed using a Zwick Z50 universal loading machine, while tests at applied remote strain rates of 10 s^{-1} and 100 s^{-1} were conducted by SHPB loading as illustrated in Fig. 2c. The details of the SHPB used can be found in Ref. [24]; it comprised a Ti64 projectile of 16 mm diameter and length of 2.7 m, and two input and output bars made from the same alloy and having length of 2.7 m and diameter of 16 mm. A pulse shaper was used in selected experiments to adjust the shape of the incoming loading pulse [23,25]. Strain gauges were attached to the bars to measure the transient longitudinal stress waves, from which the input and output forces acting on the two pistons of the apparatus could be calculated using one-dimensional stress wave theory (see for example [26]).

2.3. Data analysis

In the dynamic test, the forces exerted by the input and output bars on the apparatus can be calculated as

$$\begin{cases} F_{input} = EA[\varepsilon_I(t) + \varepsilon_R(t)] \\ F_{output} = EA\varepsilon_T(t) \end{cases} \tag{1}$$

where EA represents the axial stiffness of the input and output bars, ε is the transient strain in the bar and subscripts *I, R, T* stand for incident, reflected and transmitted waves, respectively, and are obtained by a wave separation technique [26]. After a brief transient the input and output forces equalised (force equilibrium was reached); from this point on, the pressure in the fluid p_0 could be calculated as $p_0 = F_{input}/A_0 = F_{output}/A_0 = F/A_0$, where A_0 is the cross-sectional area of the piston. In static tests the force F was directly measured.

With reference to Fig. 3, we denote the pressure at the interface between rubber sleeve and specimen as p_i, while the (average) circumferential stress in the rubber and specimen are denoted as σ_R, σ_S, respectively. If h_R, h_S are the heights of rubber sleeve and specimen, respectively, and R_0, R_i are the inner radii of rubber sleeve and specimen, respectively, the static equilibrium of the specimen and rubber sleeve reads

$$\sigma_S A_S = p_i R_i h_S \tag{2}$$

$$\sigma_R A_R + p_i R_i h_S = p_0 R_0 h_R \tag{3}$$

where A_R, A_S are the cross-sectional areas of rubber sleeve and specimen, respectively. The hoop stress in the specimen is

$$\sigma_S = \frac{1}{A_S}\left[\frac{R_0 h_R F}{A_0} - A_R \sigma_R(\varepsilon)\right]. \tag{4}$$

The simple analysis above neglects all inertial and frictional forces. We showed in detail in Ref. [21] that this is a good approximation, which applies to the tests conducted in this study; details of the effects of friction and inertia can also be found in Refs. [20–23]. The term $\sigma_R(\varepsilon)$, denoting the constitutive response of the rubber sleeve material, can be measured by performing tests with the specimen absent, as shown in Refs. [20–23]. The term in eq. (4) containing $\sigma_R(\varepsilon)$ can often be

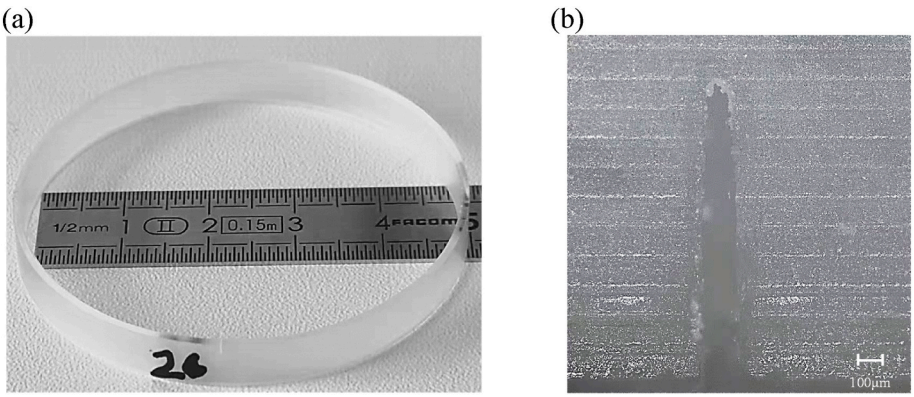

Fig. 1. (A) Example of a cracked PMMA ring specimen; (b) Example of the optical micrographs used for the measurement of the initial crack length.

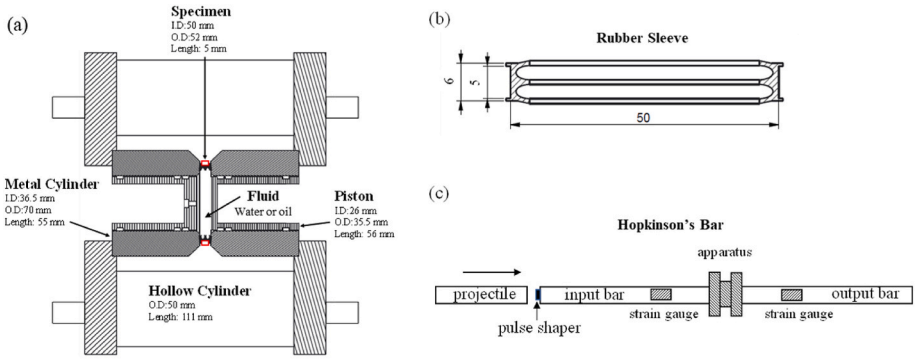

Fig. 2. (A) Cross-sectional view of the apparatus, reproduced from Ref. [21]; (b) cross-section of the rubber sleeve supporting the specimen; (c) sketch of the arrangement of the test apparatus in the SHPB setup.

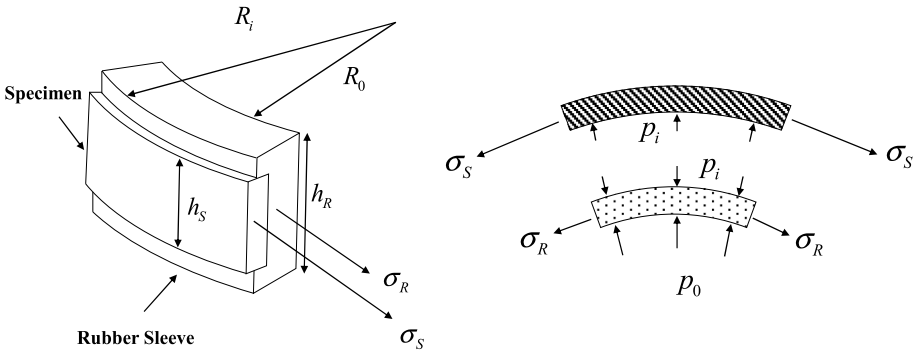

Fig. 3. Geometry and free-body diagram of the active part of the apparatus.

neglected in comparison to $R_0 h_R F/A_0$, such that

$$\sigma_S(t) = \frac{R_0 h_R F(t)}{A_0 A_S}; \tag{5}$$

However, in this study, we use eq. (4) to calculate the remote hoop stress in the specimen, due to the high hoop compliance of the relatively soft PMMA specimens used.

In the case of specimens containing cracks, as those tested here, $\sigma_S(t)$ is taken as the remotely applied stress at sufficiently large distance from the crack, while ε_S denotes the remote hoop strain (applied at sufficient distance from the crack). The rate of strain in the circumferential direction $\dot{\varepsilon}_S(t)$ can be readily measured by a strain gauge oriented in the circumferential direction.

We note here that both $\dot{\varepsilon}_S(t)$ and $\sigma_S(t)$ vary in time but are uniform in space at sufficient distance from the crack. This allows a clear definition of the imposed strain rate in the fracture experiments. The uniformity of the stress field results in the fact that the Mode I stress intensity factors can be calculated using formulae derived for quasi-static scenarios, namely

$$K_I = \beta \sigma_S \sqrt{\pi a} \tag{6}$$

where a is the crack length and β is a dimensionless quantity accounting for the problem geometry, found in Ref. [27] and reading

$$\beta\left(\frac{a}{H}\right) = 1.12 - 0.231\frac{a}{H} + 10.55\left(\frac{a}{H}\right)^2 - 21.710\left(\frac{a}{H}\right)^3 + 30.382\left(\frac{a}{H}\right)^4 \tag{7}$$

The condition for fracture is therefore

$$\sigma_S^* = \frac{K_{Ic}}{\beta(a/H)\sqrt{\pi a}}. \tag{8}$$

with the asterisc denoting quantities measured at fracture. We note that when the quasi-static expressions for the stress intensity factor above are used in dynamic tests, one typically checks that the loading time to failure clearly exceeds the time needed for a stress wave to travel a distance equal to the crack length. This check is satisfied in this study, as the wave speed of PMMA was measured indirectly as approximately 1740 m/s, the largest crack length used is 1.22 mm (hence the wave travel time is of order 700 ns), and the maximum loading time in dynamic tests exceeds 50 ms. This check however might be not necessary for this method, which does not involve stress waves travelling in the plane of the specimens.

3. Results and discussion

Table 1 summarises the details of the experiments conducted in this study. The applied remote strain rate was directly measured in selected tests (where a strain gauge was used) or estimated as $\dot{\varepsilon}_S = VA_0/(2\pi R_i^2 h_R)$, following from conservation of volume, upon assuming incompressibility of rubber sleeve and water [21]. V was taken as the (measured) velocity of the piston; in dynamic tests, this was evaluated at the point of force equilibrium. The table shows that experiments were conducted at strain rates of order of magnitude 10^{-3}, 10 and 100 s^{-1}.

For each value of the crack length we report the remote stress at fracture and the corresponding value of the fracture toughness K_{Ic}, calculated from eq. (6) making use of the relevant value of a/H.

In all tests (including the quasi-static ones) the material response was brittle, with the crack propagating unstably in the direction of the height of the specimen and creating a smooth fracture surface.

Fig. 4a shows the stress versus strain response of three specimens with no cracks at different strain rates, to highlight the material's strain rate sensitivity. At all strain rates the material displays a nonlinear, monotonically increasing response. The point of force equilibrium in the dynamic tests is indicated by circles. The stiffness and strength of the material increase considerably with increasing strain rate, while the strain to failure decreases, in line with the findings of [21]. This suggests the presence of two competing mechanisms affecting the sensitivity of

Table 1
Summary of the test results (add a column with strain rate as described above).

strain rate (order of magnitude) $\dot{\varepsilon}_S$ (s^{-1})	strain rate $\dot{\varepsilon}_S$ (s^{-1}) (measured) or estimated	crack length a (mm)	a/H	remote fracture stress σ_S^* (MPa)	fracture toughness K_{Ic} (MPa $m^{1/2}$)
10^{-3}	(0.001)	0	0	95	N/A
	0.001	0.21	0.042	60	1.78
	0.001	0.27	0.054	51	1.69
	0.001	0.39	0.078	46	1.86
	0.001	0.46	0.092	43	1.94
	0.001	0.62	0.124	40	2.15
	(0.0006)	0.85	0.170	31	2.06
	0.001	1.22	0.244	30	2.74
10	(14)	0	0	139	N/A
	13	0.25	0.050	79	2.53
	5	0.35	0.070	71	2.72
	11	0.48	0.096	54	2.50
	(9)	0.75	0.150	43	2.63
	9	0.98	0.196	43	3.24
	10	1.06	0.212	43	3.46
10^2	(78)	0	0	150	N/A
	73	0.21	0.042	108	3.13
	(108)	0.30	0.060	97	3.40
	75	0.44	0.088	73	3.18
	100	0.60	0.120	66	3.50
	80	0.82	0.164	61	4.02
	102	1.01	0.202	53	4.09
	78	1.10	0.220	54	4.52

the material's fracture toughness to the applied strain rate.

In Fig. 4b we plot, for selected specimens tested at the three different strain rates, the history of the stress intensity factor as a function of the applied remote strain; this suggests that the fracture toughness increases with increasing strain rate, as it is also evident from the data in Table 1. The points of force equilibrium in the dynamic tests are indicated by the two circles. We note that despite the very small strains to failure, our experimental technique allows valid stress versus strain measurements and therefore valid measurements of K_{Ic}. This is typically not the case in previous studies, particularly when dealing with brittle solids.

In Fig. 4c we show the variation of the remote fracture stress σ_S^* as a function of a/H; the figure includes a least squares fit of eq. (8) through the datapoints, consistent with the notion that the fracture toughness K_{Ic} is a material property independent of a/H but only dependent on the applied strain rate $\dot{\varepsilon}_S$. As expected, eq. (8) has initial slope of $-1/2$ in double logarithmic space, while this slope is modified, at increasing a/H, by the geometric correction function β. Equation (8) fits the data well at relatively small values of a/H, but underestimates the remote fracture stress at high values of a/H. The reasons for this are not investigated further here and might be related to slightly different modes of deformation in proximity of the crack, related to the large crack lengths. For example, 3D deformation effects may become more prominent in the vicinity of the crack, effectively changing the stress intensity factor. This conjecture is motivated by the fact that visual observation during the

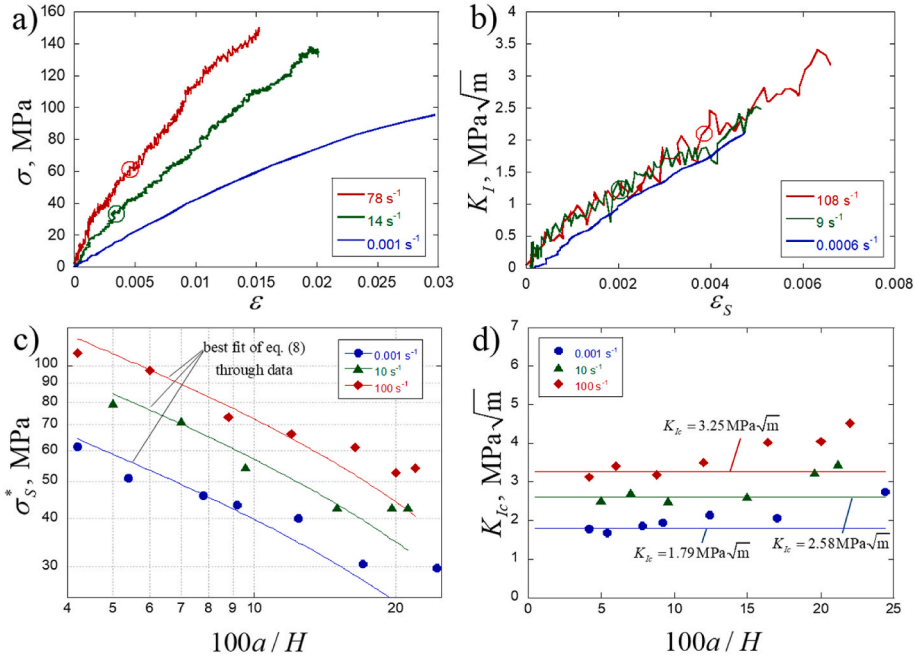

Fig. 4. (A) Stress versus strain responses of specimens with no cracks at different strain rates; (b) Evolution of the stress intensity factor at different strain rates (a/H of 0.17, 0.15, 0.06 for specimens tested at rates of 0.0006, 9, 108 s^{-1}, respectively); (c) Dependence of the fracture stress upon a/H at different rates; (d) Dependence of the measured fracture toughness upon initial crack length and strain rate.

Table 2
Comparison of the measurements in this study to previously published data.

	K_{Ic}^0(MPa$\sqrt{\text{m}}$)	exponent N (eq. (9))	min. Rate tested, s^{-1}	max. Rate tested, s^{-1}	Force equil. Checked
Present paper	1.79	0.049	0.001	100	YES
Ref. [6]	0.001	0.782	15	60	NO
Ref. [8]	1.59	0.037	0.0001	1000	NO

static tests suggested a slightly more prominent bulging of the rubber sleeve in the region of the crack. Fitting eq. (8) through the entire dataset yields values of K_{Ic} of 1.87, 2.67 and 3.40 MPa$\sqrt{\text{m}}$ at strain rates of order 10^{-3}, 10, 10^2 s^{-1}, respectively. To remove the possibly problematic tests at large a/H, the fitting of eq. (8) through the data is repeated by considering, at each strain rate, only the four smallest values of a/H. This yields marginally lower values of K_{Ic} of 1.79, 2.58 and 3.25 MPa$\sqrt{\text{m}}$ at strain rates of 10^{-3}, 10, 10^2 s^{-1}, respectively.

These values of K_{Ic} are indicated as horizontal lines in Fig. 4d, which also reports the individual measurements of K_{Ic} from Table 1. To quantify the sensitivity of K_{Ic} to the applied strain rate, and to compare to previous measurements in the literature, the three datapoints are fitted by the power-law

$$K_{Ic} = K_{Ic}^0 \left(\frac{\dot{\varepsilon}_S}{\dot{\varepsilon}_S^0} \right)^N, \tag{9}$$

where K_{Ic}^0 is an experimental constant, broadly representative of the fracture toughness at the reference strain rate $\dot{\varepsilon}_S^0$, chosen as $\dot{\varepsilon}_S^0 = 10^{-3}$ s^{-1}. The exponent N quantifies the sensitivity of K_{Ic} to $\dot{\varepsilon}_S$. A comparison of our measurements to those previously appeared in the literature is shown in Table 2. We note that only two of the papers reviewed reported the sensitivity of K_{Ic} to $\dot{\varepsilon}_S$..

The constant K_{Ic}^0 determined in this study is higher than the quasi-static fracture toughness reported in Refs. [1,5,7] and this is consistent with the fact that in these studies a plane-strain fracture toughness is obtained, while our experiments are closer to the plane-stress idealisation, due to the thin specimens used; the difference however could also partly be ascribed to the variability in the mechanical response of PMMA produced by different routes. The exponent N determined from our tests suggests a higher sensitivity of K_{Ic} to $\dot{\varepsilon}_S$ than that reported in Ref. [8]. The sensitivity determined in Ref. [6] appears disproportionately high, considering the narrow ranges of strain rates investigated. We note however that in both [6,8], in which PMMA beams were loaded by the SHPB apparatus, force equilibrium was not checked (and therefore, possibly not achieved). Another problem in Refs. [6,8] is the definition of the applied strain rate: this was measured by optical methods (and hence affected by the limited resolution of these) at a point arbitrarily close to the crack tip; such strain rate is therefore very different from the remotely applied strain rate reported in the present study, where $\dot{\varepsilon}_S$ is clearly defined and directly measured by a strain gauge far from the crack. In other studies on the dynamic fracture toughness of PMMA, such as [1,5,8,9], the applied strain rate is not defined at all, and authors simply plot the dependence of K_{Ic} upon the stress intensity factor rate $\dot{K}_I$, resulting in datasets which depend on geometry and have narrow applications. To allow a comparison of our measurements with others appeared in the literature, we included in the Appendix a plot of our measurements of K_{Ic} upon the stress intensity factor rate $\dot{K}_I$.

We note that the Young's moduli of the material at the three strain rates investigated, measured as the initial slope of the stress versus strain curves at the point of force equilibrium, were 3.85, 6.52 and 9.62 GPa at strain rates of 10^{-3}, 10, 10^2 s^{-1}, respectively. These, together with the values of K_{Ic} from Fig. 4d, allow estimating the Mode I, plane-stress fracture energies G_{Ic} of PMMA as 0.832, 1.021 and 1.097 kJ/ m^2 at strain rates of 10^{-3}, 10, 10^2 s^{-1}, respectively. This information, which cannot be obtained from current dynamic fracture test techniques, finds direct and immediate application in numerical simulations of the dynamic fracture response of PMMA components.

We note on passing that mixed-mode fracture experiments (Modes I/II) can be easily conducted with the proposed technique, by testing specimens with initial cracks inclined at different angles with respect to the direction of the height H. This is left as a topic for future studies.

4. Concluding remarks

We proposed and assessed a new experimental technique to measure the sensitivity of the fracture toughness of solids to the applied strain rate. This technique, based on the dynamic expansion of thin-walled ring-shaped specimens, presents several advantages over those appeared to date: (i) it results in spatially uniform remote stress and strain fields, allowing a clear definition of the remotely applied stress and strains and of the stress intensity factors; (ii) it allows applying high strain rates, using the same specimen and setup at all strain rates; (iii) when used with a SHPB apparatus, it results in early force equilibrium and valid force measurements even for very brittle solids; (iv) the test rig is compact and it is suitable for measurements in conditioned environments.

We applied the technique to measure the sensitivity of K_{Ic} and G_{Ic} to the applied remote strain rate, obtaining a dataset immediately applicable in the numerical simulation of the response of PMMA components subject to highly dynamic loads. The measured data shows an increase in fracture toughness with increasing strain rate. In quantitative terms, our measurements are different from those previously published, and arguably more accurate, as they eliminate several problems in these types of experiments.

Author statement

Junyi Zhou: Investigation; Data curation; Formal analysis; Writing – original draft. Antonio Pellegrino: Funding Acquisition; Supervision: Writing – review & editing. Vito Tagarielli: Conceptualisation; Methodology; Writing – review & editing.

Declaration of competing interest

The authors declare that they have no known competing financial interests or personal relationships that could have appeared to influence the work reported in this paper.

Data availability

Data will be made available on request.

Acknowledgements

We acknowledge the assistance of Stuart Carter (Oxford) in the manufacturing and instrumentation of all specimens. The research is supported by Rolls-Royce plc and EPSRC under the Prosperity Partnership Grant\Cornerstone: Mechanical Engineering Science to Enable Aero Propulsion Futures, Grant 512 Ref: EP/R004951/1.

APPENDIX. Fracture toughness as a function of the stress intensity factor rate

Our proposed technique allows relating K_{Ic} to the remotely applied strain rate, which is clearly defined in the present tests, and for this reason our measurements are presented as a function of the remote applied strain rate in Fig. 4, eq. (9) and Table 2. However in the majority of other studies in the literature, in which such strain rate could be clearly identified, researchers have plotted K_{Ic} as a function of the stress intensity factor rate $\dot{K}_I$. To allow a direct comparison with the data in the literature Figure A1 presents our measured fracture toughness as a function of $\dot{K}_I$.

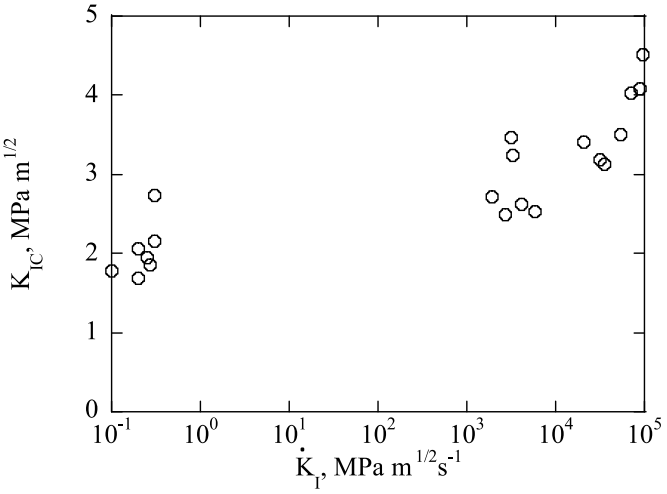

Fig. A1. Fracture toughness of PMMA at different stress intensity factor rates.

References

[1] A. Faye, V. Parameswaran, S. Basu, Dynamic fracture initiation toughness of PMMA: a critical evaluation, Mech. Mater. 94 (2016) 156–169.
[2] T.M. Maccagno, J.F. Knott, The fracture behaviour of PMMA in mixed modes I and II, Eng. Fract. Mech. 34 (1) (1989) 65–86.
[3] M.R.M. Aliha, A. Bahmani, S. Akhondi, Mixed mode fracture toughness testing of PMMA with different three-point bend type specimens, Eur. J. Mech. Solid. 58 (2016) 148–162.
[4] F. Jiang, K.S. Vecchio, Hopkinson bar loaded fracture experimental technique: a critical review of dynamic fracture toughness tests, Appl. Mech. Rev. 62 (6) (2009).
[5] W. Hitoshi, Determination of dynamic fracture toughness for PMMA, Eng. Fract. Mech. 41 (6) (1992) 821–831.
[6] W. Zhou, J. Huang, W. Huang, D. Liu, Dynamic fracture testing of polymethyl-methacrylate (PMMA) single-edge notched beam, Polym. Test. 91 (2020), 106833.
[7] T. Weerasooriya, P. Moy, D. Casem, M. Cheng, W. Chen, Fracture toughness for PMMA as a function of loading rate, in: Proceedings of the 2006 SEM Annual Conference & Exposition on Experimental and Applied Mechanics, 2006, June.
[8] S. Sahraoui, J.L. Lataillade, Deformation and fracture of PMMA at high rates of loading, J. Appl. Polym. Sci. 51 (9) (1994) 1527–1532.
[9] J. Zhou, Y. Wang, Y. Xia, Mode-I fracture toughness of PMMA at high loading rates, J. Mater. Sci. 41 (24) (2006) 8363–8366.
[10] Y.X. Zhou, K.W. Xia, X.B. Li, H.B. Li, G.W. Ma, J. Zhao, Z.L. Zhou, F. Dai, Suggested methods for determining the dynamic strength parameters and mode-I fracture toughness of rock materials, in: The ISRM Suggested Methods for Rock Characterization, Testing and Monitoring, Springer, Cham, 2012, pp. 35–44, 2007-2014.
[11] fish 0,punct]"> W. Yao, K. Xia, Dynamic notched semi-circle bend (NSCB) method for measuring fracture properties of rocks: fundamentals and applications, J. Rock Mech. Geotech. Eng. 11 (5) (2019) 1066–1093.
[12] C.R. Hoggatt, R.F. Recht, Stress-strain data obtained at high rates using an expanding ring, Exp. Mech. 9 (10) (1969) 441–448.
[13] R.H. Warnes, R.R. Karpp, P.S. Follansbee, The freely expanding ring test-a test to determine material strength at high strain rates, Transac. ASME.J. Eng. Mater. Technol. 108 (4) (1986) 335–339.
[14] N. Al-Maliky, D.J. Parry, Measurements of high strain rate properties of polymers using an expanding ring method, J. Phys. IV : JP. 4 (8) (1994). C8-71-C8-76.
[15] H. Zhang, K. Ravi-Chandar, On the dynamics of necking and fragmentation - I. Real-time and post-mortem observations in Al 6061-O, Int. J. Fract. 142 (3–4) (2006) 183–217.
[16] H. Zhang, K. Ravi-Chandar, On the dynamics of necking and fragmentation - II. Effect of material properties, geometrical constraints and absolute size, Int. J. Fract. 150 (1–2) (2008) 3–36.
[17] H. Zhang, K. Liechti, K. Ravi-Chandar, On the dynamics of localization and fragmentation. III. Effect of cladding with a polymer, Int. J. Fract. 155 (2) (2009) 101–118.
[18] H. Zhang, K. Ravi-Chandar, On the dynamics of localization and fragmentation-IV. Expansion of Al 6061-O tubes, Int. J. Fract. 163 (1–2) (2010) 41–65.
[19] R. Chen, Z.Y. Nie, Y. Peng, Y. Xu, W. Yao, A dynamic hydraulic fracturing test technology based on split Hopkinson pressure bar system, Exp. Mech. (2022) 1–10.
[20] J. Zhou, V.L. Tagarielli, U. Heisserer, P.T. Curtis, An apparatus for tensile testing of engineering materials, Exp. Mech. 58 (6) (2018) 941–950.
[21] J. Zhou, A. Pellegrino, U. Heisserer, P.W. Duke, P.T. Curtis, J. Morton, N. Petrinic, V.L. Tagarielli, A new technique for tensile testing of engineering materials and composites at high strain rates, Proc. Royal Soc. A 475 (2229) (2019), 20190310.
[22] J. Zhou, U. Heisserer, P.W. Duke, P.T. Curtis, J. Morton, V.L. Tagarielli, The sensitivity of the tensile properties of PMMA, Kevlar® and Dyneema® to temperature and strain rate, Polymer 225 (2021), 123781.
[23] J. Zhou, V.L. Tagarielli, On the development of new test techniques to measure the tensile response of materials at high and ultra-high strain rates, Exp. Mech. (2021) 1–14.
[24] A. Pellegrino, V.L. Tagarielli, R. Gerlach, N. Petrinic, The mechanical response of a syntactic polyurethane foam at low and high rates of strain, Int. J. Impact Eng. 75 (2015) 214–221.
[25] Y.B. Lu, Q.M. Li, Appraisal of pulse-shaping technique in split Hopkinson pressure bar tests for brittle materials, Int. J. Prot. Struct. 1 (3) (2010) 363–390.
[26] V.L. Tagarielli, V.S. Deshpande, N.A. Fleck, The high strain rate response of PVC foams and end-grain balsa wood, Compos. B Eng. 39 (1) (2008) 83–91.
[27] H. Tada, P.C. Paris, G.R. Irwin, The Stress Analysis of Cracks, vol. 34, Del Research Corporation, Handbook, 1973.